Wear 466–467 (2021) 203571

Contents lists available at ScienceDirect

Wear

journal homepage: http://www.elsevier.com/locate/wear

Effect of niobium and molybdenum addition on the wear resistance and the rolling contact fatigue of railway wheels

A.B. Rezende *, S.T. Fonseca, R.S. Miranda, F.M. Fernandes, F.A.F. Grijalba, P.F.S. Farina, P. R. Mei

University of Campinas, School of Mechanical Engineering, 13083-860, Campinas, SP, Brazil

ARTICLE INFO

Keywords:
Twin-disc test
Wear
Rolling contact fatigue
Niobium
Molybdenum
Magnetic Barkhausen noise
Microalloyed steel
Railway wheel

ABSTRACT

Brazilian heavy-haul railway companies have drawn extensive research in the last years for developing solutions that can make the operation in this area more efficient and safer, such as friction management, the use of new mechanical assemblies, and the use of new materials for wheels and rails. Another solution implemented is increasing the weight transported by train wagons; however, the more weight added, the more deterioration caused to wheels and rails, for example, promoting higher maintenance costs and risks to safety. Thus, the key to extending the life cycle of railroad wheels is to reduce the wear and rolling contact fatigue (RCF) in developing new materials and in manufacturing them. Niobium (Nb) and molybdenum (Mo) are usually added to increase the mechanical strength of pearlitic steels by decreasing the interlayer spacing. This way, comparative twin-disc test for wheel material under dry conditions was performed to verify the wear resistance of a commercial railway wheel (7C) and a newly developed class D railway wheel steel (7 M) with Nb and Mo addition. Following the specifications of the Association of American Railroads (AAR) standard, a twin-disc tribometer with automatic control of load and speed was used. The slip ratio was obtained from the difference between the axis rotation. 7 M steel was observed to present lower mass loss compared with 7C steel. The Magnetic Barkhausen noise analysis showed higher residual stress close to the surface for 7 M steel, which correlated with the work-hardened depth. Such results, therefore, indicate that 7 M steel presented better performance than 7C steel regarding the specific characteristics of the tests. To confirm the feasibility of the wheel material for use in service, further twin-disc tests are proposed for both wheel materials (7 M & 7C) against the same rail material.

1. Introduction

Brazilian heavy-haul railway companies have been making transport more efficient by increasing the weight transported. However, this weight addition leads not only to damaged components but also to premature wear and safety risks. Failures caused by wear and rolling contact fatigue (RCF) on wheels and rails are inevitable operational problems on the trackways as a result of high stress developed from the contact of these two elements [1–4]. Bevan et al. [5] mapped out the incidence of these two types of damage in the profiles of railroad wheels used, and determined the categories of the ones that mainly occur. The results indicated that 41% of them corresponded to RCF and 26% referred to tread wear within the set of wheel failure modes.

Although rails and wheels have well-developed maintenance schedules (e.g. wheel reprofiling or rail grinding), damage to the wheel/rail surface can develop quickly. Therefore, due to such damage, sometimes they have to be prematurely removed to be repaired or even replaced [5–7], which leads to a negative impact on service provision for a railway fleet, as well as high costs generated in the replacement of vehicle and trackway components [8]. Thus, continuous improvement of materials for this application is necessary [3] because of the nucleation of surface and subsurface cracks [9], the high rates of superficial plastic deformation [10], and the severe multiaxial state of stress in the contact region during rolling [11].

A very effective way to achieve the improvement of mechanical properties is through the elaborate design of the chemical composition [12,13]. The addition of alloy elements in railway steels, such as the content of carbon (C), molybdenum (Mo), niobium (Nb), and vanadium (V) – combined with a thermal or thermomechanical treatment to obtain a quite refined structure of pearlite – favors the gain of tensile strength and improved properties of wear and fatigue [14–18].

Nevertheless, higher C content can impair the mechanical properties

* Corresponding author.
E-mail address: andreibavaresco@gmail.com (A.B. Rezende).

https://doi.org/10.1016/j.wear.2020.203571
Received 1 July 2020; Received in revised form 9 November 2020; Accepted 29 November 2020
Available online 3 December 2020

Table 1
Chemical composition of the steels used in this study (% mass).

Steel	C	Si	Mn	P	S	Nb	Mo
7C	0.68	0.34	0.83	0.013	0.010	–	–
7 M	0.77	0.28	0.86	0.017	0.022	0.023	0.25

and cause the formation of proeutectoid cementite in prior austenite grain boundaries, which can impact the fracture toughness and make the formation of cracks in the grain boundaries more likely to occur; consequently, wear and RCF behavior are affected [12,19]. Hence, it is clear that a good combination and the right amounts of alloy and microalloyed elements (Mo, V, Nb, manganese (Mn), etc.) are the key to optimizing the wear and fatigue properties of railway steels [20,21]. Therefore, the authors asserted that research efforts are crucial to determine the best combination of composition and microstructure so that it is possible to produce steels with optimized performance on the railroad, once studies have been presenting bainitic steels as potential replacements for pearlitic steel microstructure in wheel and rail materials [22–25].

Working in this line, Zambrano at al [26] conducted wear tests by sliding in the block-on-ring using 191 HV hardness steels of different compositions and microstructures (AISI 5160 pearlitic and AISI 1045 ferritic-pearlitic). The group found that fully pearlitic steel had the best wear resistance, and they credited this behavior to its microstructure. Qiu at al [21] affirmed that the composition of new heavy-haul railroad wheel steels with adequate Nb and V concentrations benefits the RCF performance, and Mo contents could act on stability, improving the perlite. Solano-Alvarez et al. [27] carried out dry twin-disc wear tests of two commercial pearlitic steels with and without V addition for application in light-weight rails. The results indicated that V alloyed steel presented a wear rate two times lower than the alloy without this element. Other authors also concluded that V and Nb addition could improve the wear and RCF properties of pearlitic steels [28,29]. On the other hand, Godefroid et al. [30] performed fracture toughness and crack propagation tests with two steels with and without V addition. The authors concluded that the two steels exhibited similar fracture toughness, and that steel without V showed greater resistance to fatigue crack growth. This way, the common steel would be the most economically viable option and with the best fatigue performance for railway

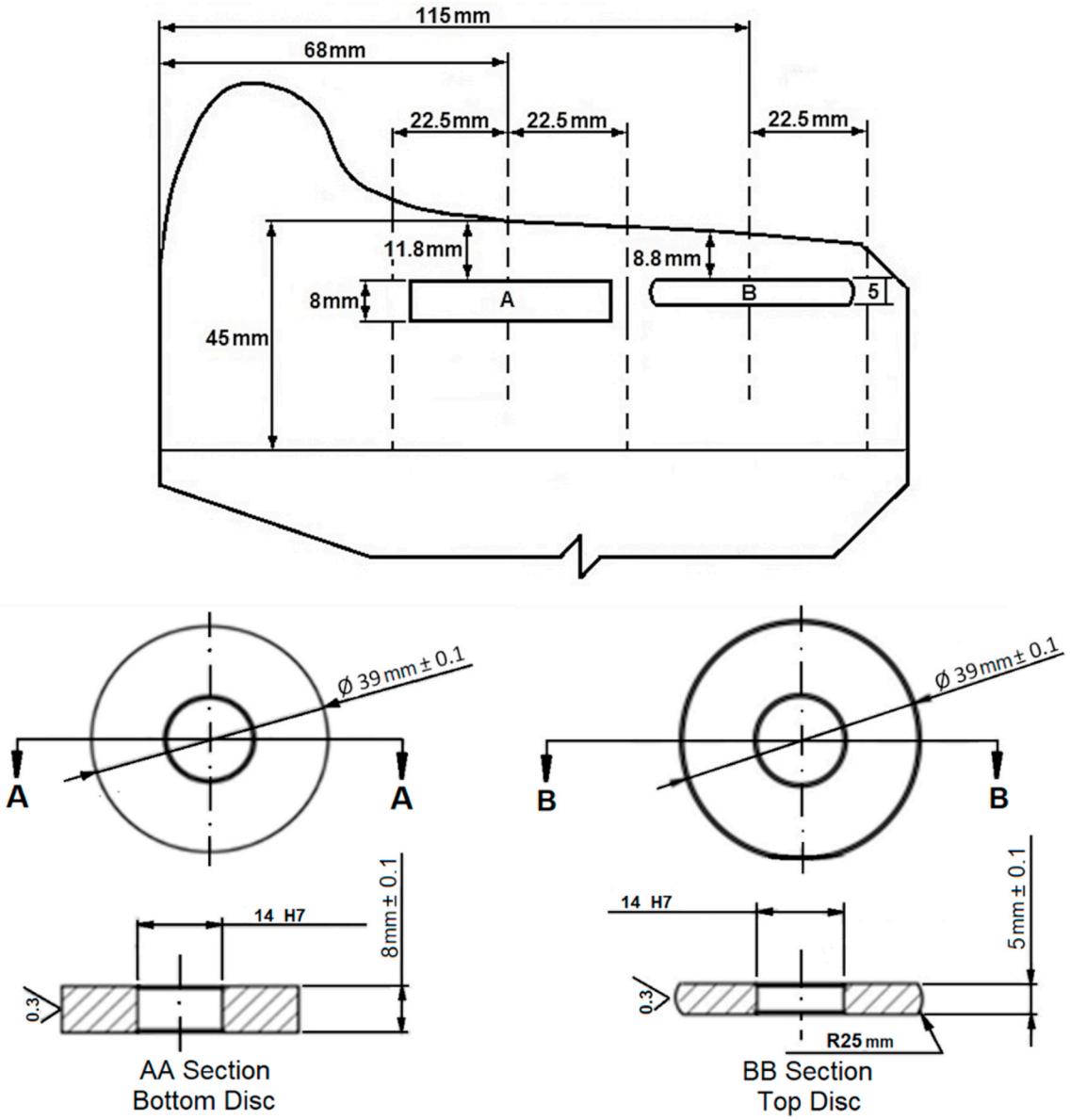

Fig. 1. a) Position in the wheel from which the discs were removed (in millimeters); b) Dimension of the discs used in the twin-disc tribometer (in millimeters).

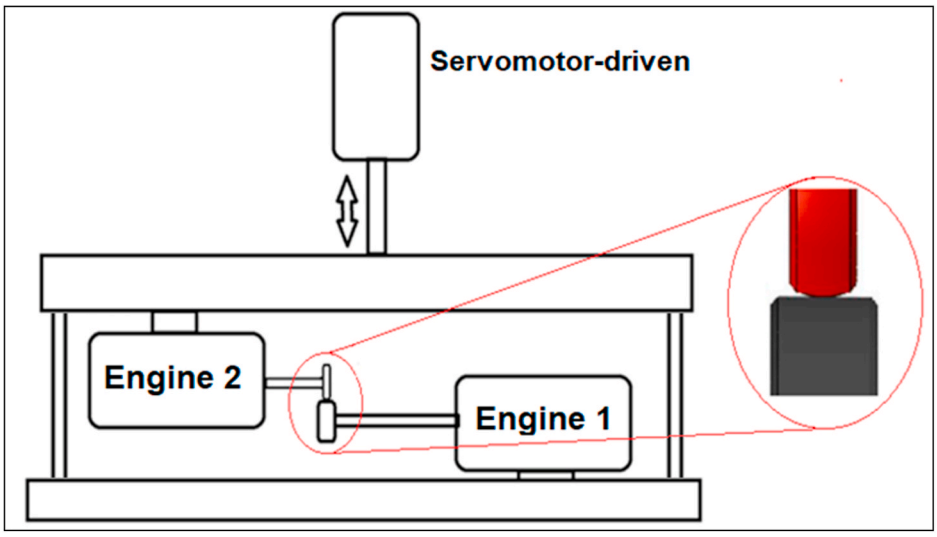

Fig. 2. Schematic representation of the twin-disc wear machine [34].

Table 2
Parameters of the twin-disc tribometer.

Load	Rotation Speed	Slip	Total Cycles
1177 N	Top Axis (B) = 168.725 rpm Bottom Axis (A) = 170 rpm	0.75%	500,000

applications.

Therefore, in view of all these facts presented, it becomes imperative to carry out the study and characterization of the wear and RCF properties of new microalloyed wheel steels in order to supply the emerging demands of the railway industry. For this purpose, with the use of a twin-disc tribometer to assess tribological properties, two railway wheel steels were analyzed: a commercial class C one (7C steel) and a recently developed class D steel with Mo and Nb addition (7 M steel). To support the characterization of the materials, measurements of microhardness, scanning electron microscopy (SEM), mass loss, and magnetic Barkhausen noise (MBN) were taken; moreover, the assessment of surface and subsurface cracks in the runway was performed.

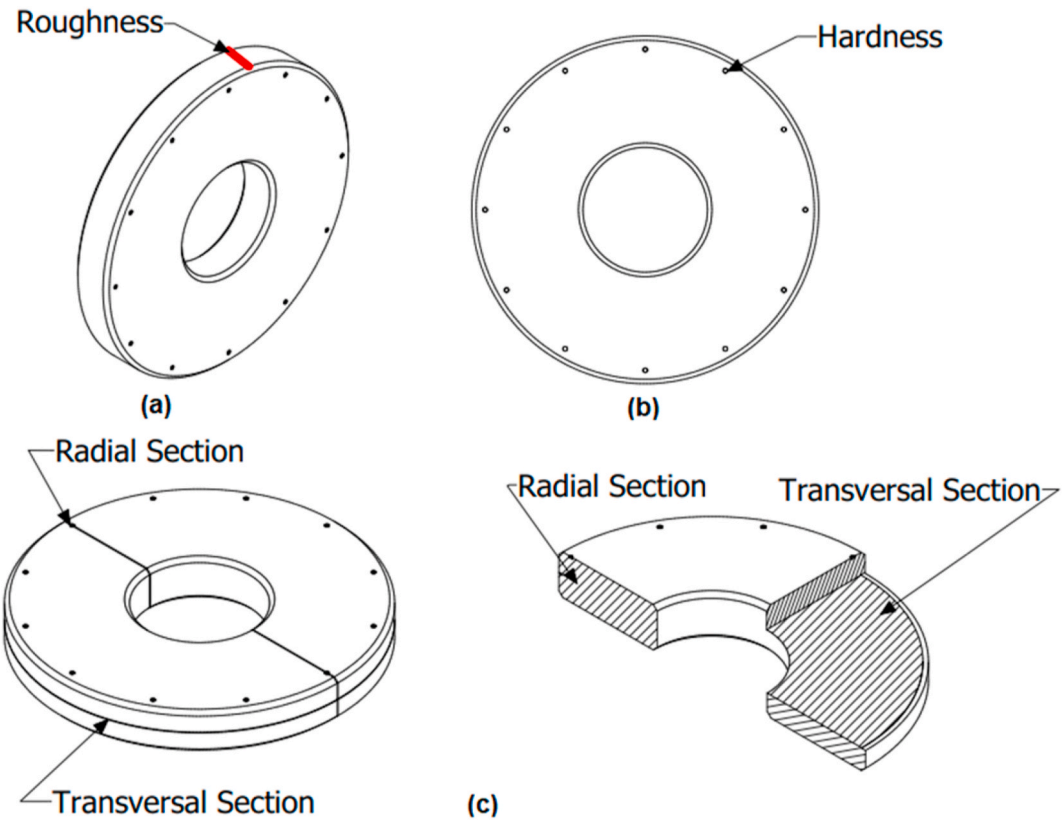

Fig. 3. Surface used for analysis: a) surface roughness, scanning electron microscopy (SEM); b) circumferential hardness on the surface of the disc; c) radial section: hardness and SEM; cross-section: optical microscopy (OM) and SEM.

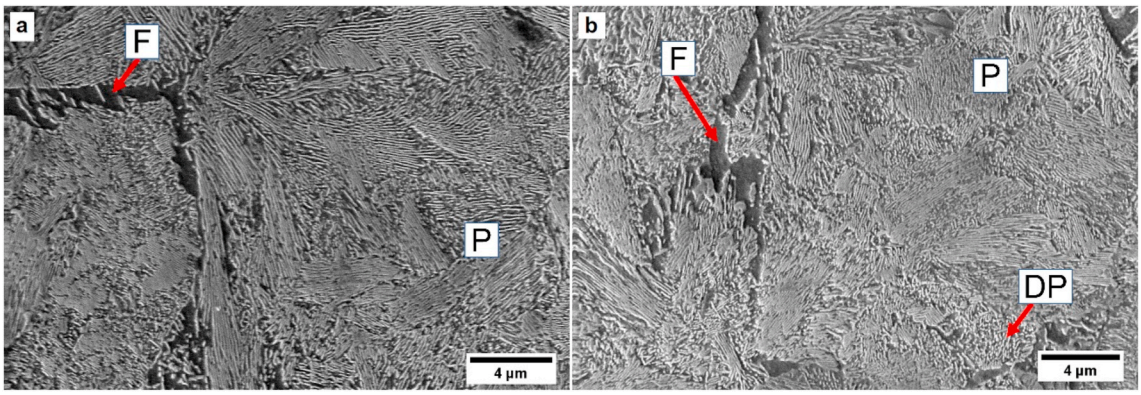

Fig. 4. Initial microstructure of the discs. a) 7CA; b) 7CB. 2% Nital. F – grain boundary ferrite; DP – degenerated pearlite; P – pearlite.

2. Materials and methods

The research was performed in the Tribology Laboratory facilities at the University of Campinas. The discs were made of two steels of forged railway wheels, and their chemical compositions (Table 1) were measured by optical spectrometry (ARL 3460 OES, Thermo Scientific). 7C steel was a conventional forged class C railway wheel, and 7 M steel was a microalloyed class D railway wheel with microaddition of elements like Mo and Nb.

The discs were removed from the wheels close to the rolling track, which is illustrated in Fig. 1-a. Such position ensures that the microstructure is similar to the first life of the wheel for both discs. The dimension of the final manufactured discs is shown in Fig. 1-b. The initial roughness (Ra) for all discs was 0.38 μm ± 0.05.

For each wheel steel, three wear tests were carried out in a twin-disc tribometer [17] (Fig. 2). All test parameters were according to those specified in the AAR (Association of American Railroads). Standard M-107/M208 [31] for the validation of new wheel classes requires that the pair of discs be removed from the same wheel. Thus, these tests are a preliminary verification of the 7 M steel performance to specific conditions. The lower and upper discs were obtained from the same wheel and were called 7CA and 7CB, respectively, for 7C steel, and 7MA and 7MB, respectively, for microalloyed steel (7 M). The tests simulated the wear with a slip ratio obtained from the difference between the axis rotation [6]. Air jet was used to remove the flakes from the disc interface. The tribometer software controlled and monitored the load applied by a servo and a spindle system, as well as the upper and lower axis speed. The parameters used in the tests are presented in Table 2. A target maximum contact pressure of 1100 MPa was established through an elliptical contact, and calculated using Hertzian theory for non-conforming geometry [32,33]. The mass and diameter of the discs were measured every 100,000 cycles.

Scanning electron microscopy (SEM) (EVO MA 15, Zeiss) was used to: i) analyze the surface (Fig. 3-a) and subsurface (Fig. 3-c); and ii) characterize the microstructure (Fig. 3-c). Microhardness was measured with a durometer (FV 800, Future Tech.), applying 0.5 kgf for 15 s in 12 circumferential points (Fig. 3-b) before the tests. After the tests, hardness was measured three times in a radial section direction (Fig. 3-c) from close to the surface until hardness reached the matrix value, applying 0.3 kgf for 15 s. A digital micrometer (IP65, Mitutoyo with a resolution of 0.001mm) was used to measure the diameter of the discs in six points. The MBN checked the state of stress for the upper discs before and after the tests in 12 points with applied field tangential to the surface of the samples using 40 Hz frequency and 0.32 A amplitude. The initial surface roughness was measured in the axial direction by a portable surface roughness tester (SJ-210-Series 178, Mitutoyo) in four points circumferentially spaced by 90° from each other.

3. Results and discussion

3.1. Material characterization

Fig. 4 illustrates the microstructure of 7CA and 7CB, which was composed of pearlite, grain boundary proeutectoid ferrite, and degenerated pearlite – whose higher volume was observed in 7CB. This microstructure was in accordance with that found by Fonseca [35] and Oliveira [36] for a class C railway wheel steel. The average Vickers hardness values were 368 ± 8 HV for 7CA and 348 ± 8 HV for 7CB. The relative hardness average between the discs (7CB/7CA) was 0.9.

Fig. 5 presents the microstructure of the 7 M discs, which was proeutectoid ferrite and degenerated pearlite for 7MA, but tempered bainite for 7MB. The average hardness values were 366 ± 2 HV for 7MA and 395 ± 2 HV for 7MB. The relative hardness average between the discs (7MB/7MA) was 1.1. It is noted that the addition of Nb and Mo changed the microstructure of the wheel, differently from 7C steel, which does not have such addition. Cunha et al. [14] simulated the forging process

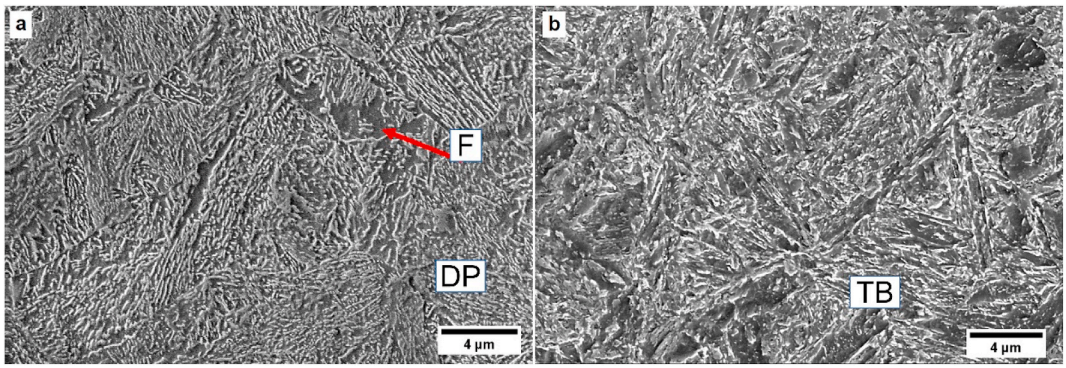

Fig. 5. Initial microstructure of the discs. a) 7MA; b) 7MB. 2% Nital. F – grain boundary ferrite; DP – degenerated pearlite; TB – tempered bainite.

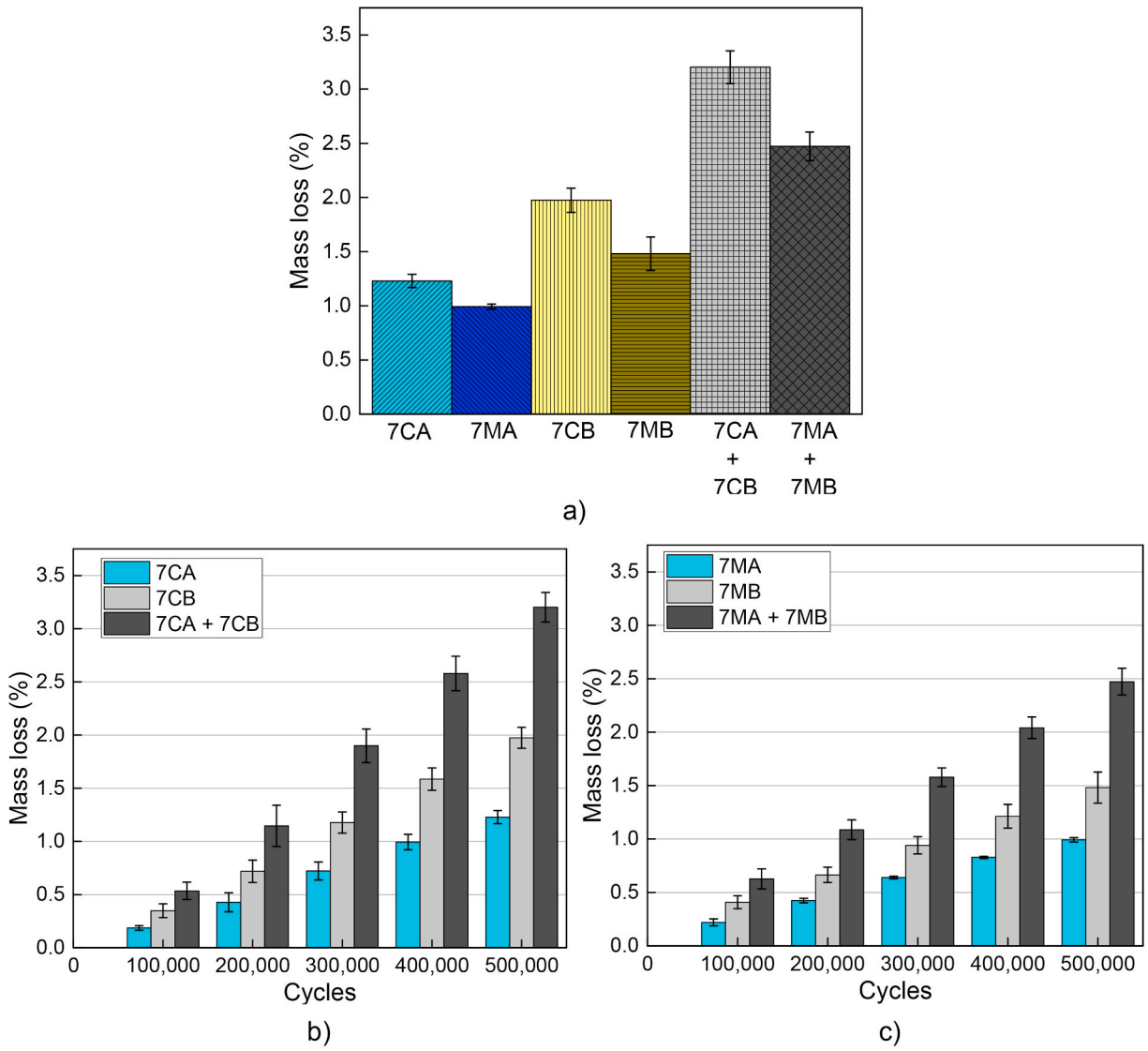

Fig. 6. Mass loss percentage after the twin-disc tests. a) 7C and 7 M discs after 500,000 cycles; b) 7CA and 7CB throughout the tests; c) 7MA and 7MB throughout the tests.

of railway wheels in steels with and without Mo and Nb addition. They found that the elements increased the tensile and yield resistance of medium carbon steel, maintaining ductility and toughness by reducing the perlite interlamellar spacing and refining the austenite grain size. According to Liu et al. [37], in high carbon pearlitic steels, the Nb atoms are incorporated into the cementite crystalline lattice, forming cementite with Nb alloy. In addition, the Nb segregation at the ferrite-cementite lamellar interface causes the solute drag effect, which generates the refinement of pearlite interlamellar spacing. Li et al. [38], working with high carbon steels with and without Nb addition, observed that Nb induces a high strengthening by solid solution and precipitation. The authors also identified that Nb increases the critical temperatures for the ferrite and perlite transformation at continuous cooling conditions. This effect is due to the refining of the austenite grain size and the presence of Nb(C, N) precipitates. The changes in the critical temperatures provide degenerated pearlite when the hot work is above eutectoid temperature, exactly as it occurs when manufacturing forged railway wheels.

Minicucci et al. [8] found a similar microstructure in class D railway wheels with the addition of Nb. According to Rezende et al. [39], the addition of Nb and Mo combined with higher C content expands the bainitic field and increases the hardenability of the railway wheel steel. Despite the fact that the heat treatment temperatures and cooling rate were the same for 7 M and 7C steel, the changes in the Continuous cooling transformation (CCT) diagram act in the microstructure and the respectively hardness. Hu et al. [40], analyzed the effect of Nb and Mo addition in carbon steels with bainitic microstructure. They found that the Nb addition delayed the austenitic transformation and that the Mo addition increased the strength of the alloy owing to the promotion of bainitic transformation.

3.2. Wear behavior

Fig. 6 shows the average mass loss for three pairs of 7C and 7 M discs after the twin-disc tests. According to Fig. 6-a, wear in 7CA was 24% higher than that in 7MA, while for 7CB it was 33% higher than for 7MB. When combining 7CA against 7CB, the pairs presented mass loss 30% greater than the 7 M pairs after 500,000 cycles (Fig. 6-a). Zhu et al. [41] detected the same trend of wear behavior for a class D steel compared with pearlitic steel. Even though 7CA and 7MA had the same hardness values, it appears that this property did not influence in their having the same mass loss. The wear rate for every 100,000 cycles was 0.64% and 0.49% in the pairs of 7C and 7 M discs, respectively. Thus, 7 M steel revealed better properties than 7C steel regarding wear. It can be seen in

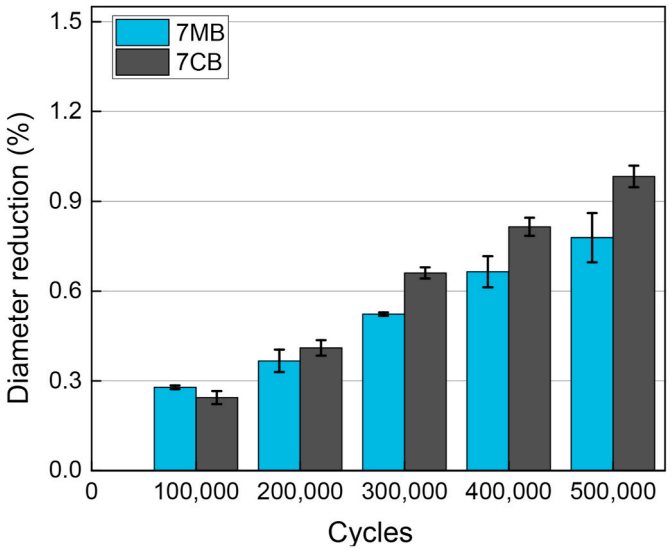

Fig. 7. Percentage of diameter reduction for the 500,000 cycles of the twin-disc tests for 7CB and 7MB discs throughout the test.

Fig. 6-b that 7CB had the highest wear throughout the test. In the first 100,000 cycles, the wear in 7CB was 85% higher than in 7CA, and it was 63% higher in the subsequent cycles. The same wear percentage between 7MA and 7MB was observed in the first 100,000 cycles, yet in subsequent cycles, the difference in mass loss was 49% (Fig. 6-c). The highest wear percentual of the lower-speed disc was also found by Zhou et al. [42]. The higher wear in the first 100,000 cycles was due to the running process [43] that increased mass loss.

Regarding diameter reduction, the measurements were taken only for the upper discs. Both 7CB and 7MB presented a linear reduction throughout the twin-disc tests, reflecting mass loss behavior (Fig. 7). However, the percentage of diameter reduction was lower than that observed for mass loss. This difference may be related to the edge deformation and an increment in the width in 7CB and 7MB as a result of the high contact load. The diameter reduction of 7CB was greater than that of 7MB after 500,000 cycles, an effect that may be associated to 7MB steel smaller mass loss, as shown in Fig. 6-a.

3.3. Worn surface

The surface analyses were carried out using one pair of discs for each steel. The worn surfaces on 7CA and 7MA are demonstrated in Fig. 8. On the surface of both discs there was a track caused by the wear, the deformation due to contact strain [42], and the non-conforming contact geometry of the discs. Disc 7CA had a slightly greater surface deterioration than did disc 7MA. The higher-magnification images evidenced the holes from the ratcheting process for both steels. Delamination with a larger number of holes on 7CA than on 7MA was observed, which, probably, contributed to the higher wear. The ratcheting mechanism is related to plastic exhaustion of the surface material caused by higher contact strain [44], and it is commonly found in other studies in the literature [6,45,46].

Fig. 9 presents the worn surface of 7CB and 7MB after the 500,000 cycles of the test. In the same way as it occurred with 7CA and 7MA, delamination and cracks were observed in both steels, as they are typical of the ratcheting mechanism. Nevertheless, 7CB and 7MB revealed a more deteriorated surface than 7CA and 7MA by virtue of the lower axial velocity in the tests [6]. The surface of 7CB steel looked more deteriorated than that of 7MB because of a larger amount of detached material promoted by the delamination process [47,48]. This characteristic contributed to 7CB greater mass loss in the wear results previously shown.

3.4. Subsurface effects

The surface and subsurface analyses were performed using the pair of discs that showed the highest wear for each steel. Fig. 10 presents the subsurface hardness profile which evaluates the plastic deformation

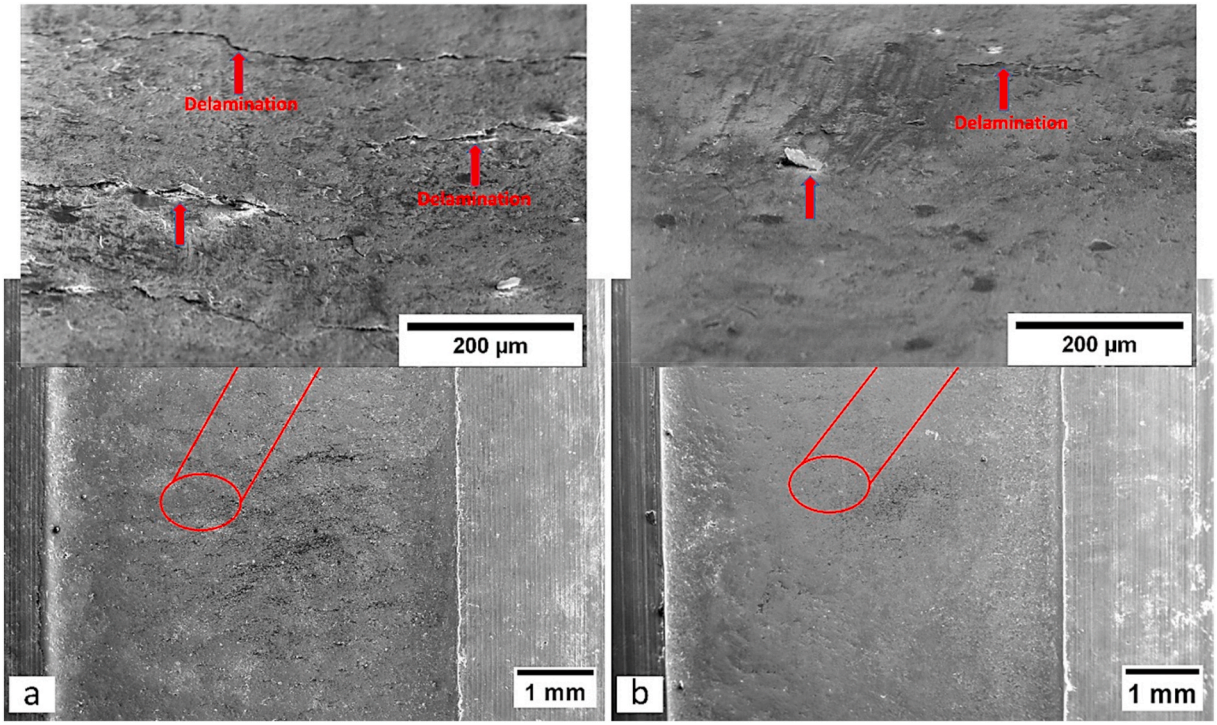

ig. 8. Morphology of the disc rolling track after 500,000 cycles. a) 7CA; b) 7MA. The red arrows indicate delamination. Scanning electron microscopy (SEM). (For interpretation of the references to colour in this figure legend, the reader is referred to the Web version of this article.)

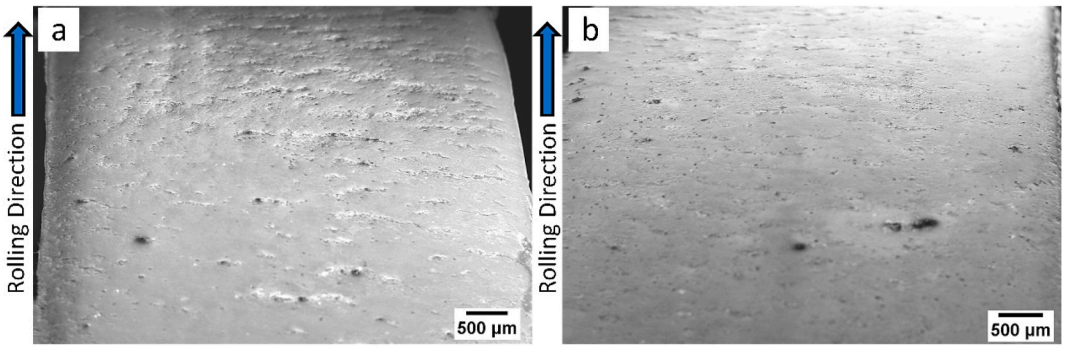

Fig. 9. Morphology of the disc rolling track after 500,000 cycles. a) 7CB; b) 7MB. Scanning electron microscopy (SEM).

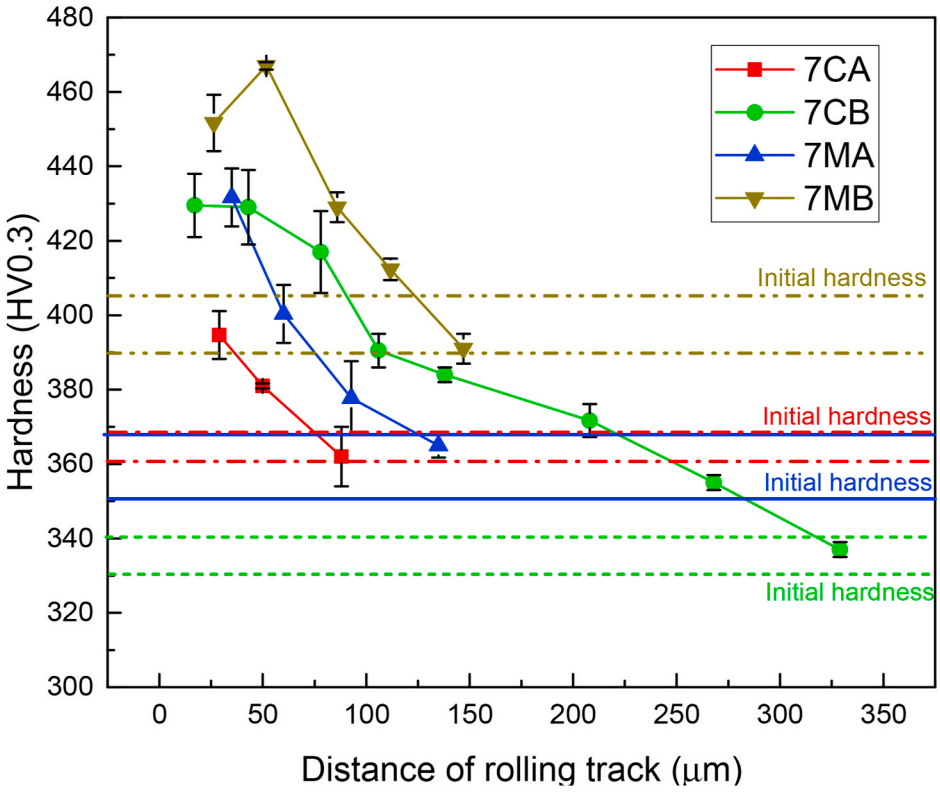

Fig. 10. Hardness profile of the cross-section of the discs.

effect below the surface of the discs. Disc 7CA reached initial hardness in 60 µm below the surface, and this one represents the shallowest deformed layer thickness among the discs studied. The depth of the deformed layer increased in the following sequence: 7MA, 7MB, and 7CB. As expected, the effect of shear force was greater on discs 7CB and 7MB than that on discs 7CA and 7MA owing to the lower speed that impacted the shear forces and the depth of the deformed subsurface layer. The highest hardness for both discs was close to the surface and gradually decreased to a certain depth at which the bulk hardness of the steel was reached, accordingly to the Hertzian theory [49,50]. At greater depths, the effect of the shear force is reduced [51,52].

After the tests, increased hardness was observed for all discs, as demonstrated in Fig. 11. By analyzing 7CA and 7MA, it was possible to notice that 7 M steel (degenerated pearlitic microstructure) had a greater hardness increment than that of 7C steel (pearlitic microstructure), which indicates a high hardening capacity of degenerated pearlite when compared to the refined structure of pearlite. Regarding 7CB and 7MB, 7C steel (pearlitic microstructure) presented a greater hardness increment than that of 7 M steel (tempered bainite). The hardening capacity of the pearlitic microstructure was higher than that of the tempered bainitic microstructure, yet this property did not increase its wear resistance. Despite presenting a smaller hardness increment than that of 7C steel, tempered bainite (7 M steel) had 18% hardening, which, combined with having smaller mass loss, makes it a better material than 7C steel in terms of wear performance.

Figs. 12 and 13 show the SEM images of 7C and 7 M steel disc cross-sections, respectively. On the surface of all discs there was severe deformation that originated cracks which spread to their subsurface, configurating the delamination process [15,53]. The angle of the cracks for 7C steel was between 6° and 9°, while for 7 M steel it was between 6° and 11° (Table 3). The results are consistent with the literature for twin-disc test with a similar 0.75% slip ratio [41,42,54]. According to Table 3, the surface cracks went to a depth of around 10 µm for 7CA, 7CB, and 7MA. Still, 7MB had much deeper surface cracks, which may produce thicker plates of removed material if they join with other cracks or emerge to the surface [55].

There were subsurface nucleated cracks that are a function of normal loading and tangential force. Energy dispersive spectroscopy (EDS)

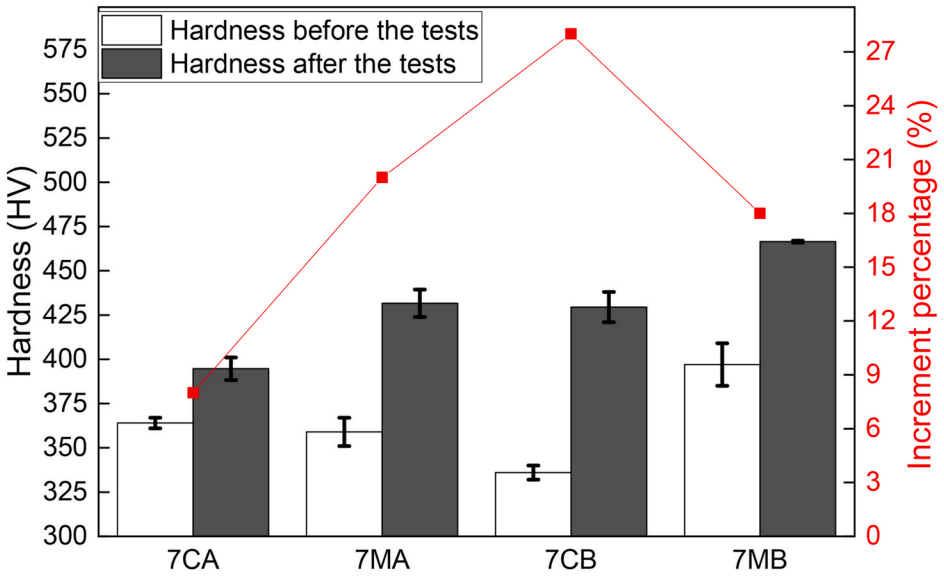

Fig. 11. Evaluation of hardness of the discs before and after the tests.

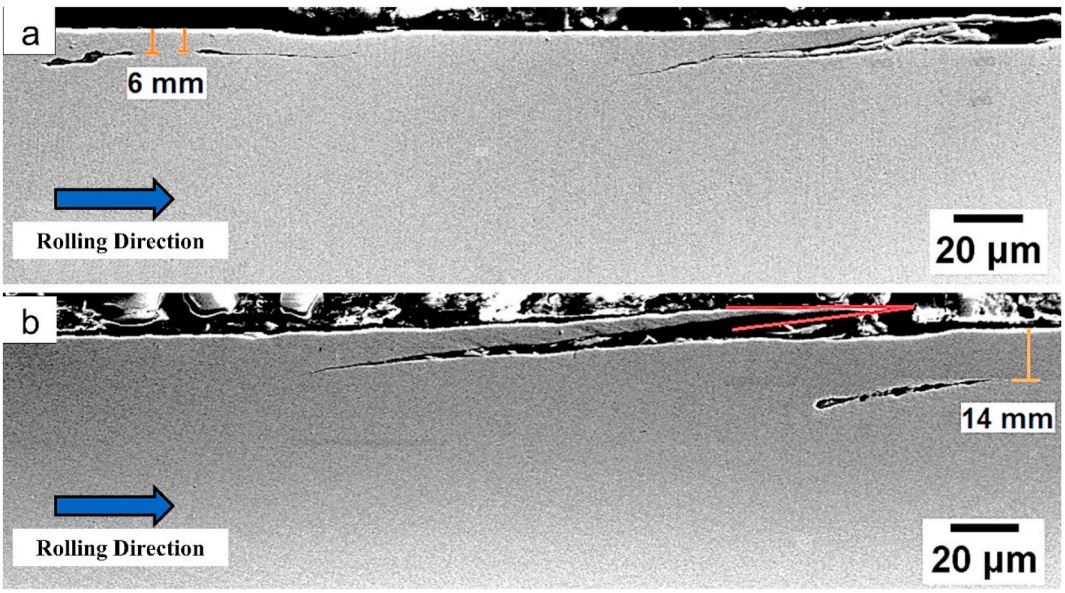

Fig. 12. Cross-section subsurface after 500,000 cycles. a) 7CA; b) 7CB. Scanning electron microscopy (SEM).

analyses indicated that such cracks started in the inclusions and voids because these hard particles act as stress concentrators [56,57]. The nucleation of the subsurface cracks was deeper in 7C steel discs than that in 7 M steel discs, and it is usually in function of the deformed layer depth [55]. As the deformed layer depth was greater in 7CB and 7MB than it was in 7CA and 7MA (Fig. 10), it was expected that the subsurface cracks started at greater depths below the rolling track.

The correlation between the mass loss percentage and depth of surface cracks is presented in Fig. 14. As the phenomenon of crack propagation is different for the upper and lower discs, they were analyzed separately. The analyses of the lower discs indicated that the deeper superficial cracks also contributed to a greater mass loss of 7CA compared with 7MA. Concerning the upper discs, a competition between wear and RCF was evidenced. In 7CB, the cracks were shallower, but the mass loss was greater. Thus, the cracks formed by cyclic plastic strain accumulation (ratcheting) were continually reduced by wear [54]. As wear was lower in 7MB, it took longer for the cracks to be removed, so they could propagate longer.

Figs. 15 and 16 present the chemically attacked cross-sectional view of the 7C steel discs. The deformed layers were considered to be accountable for the increased hardness close to the surface, as shown in Fig. 10. The depth of 7CB deformed layers was greater than that of 7CA. The deformed microstructure followed the rolling direction [58]. For both discs, lamellar pearlite was partially broken and compressed closest to the surface according to the high magnification section [59]. Nonetheless, 7CB microstructure was more brittle and compacted than 7CA microstructure, providing higher hardness. The grain boundary pro-eutectoid ferrite found in the initial microstructure was deformed and elongated because of the action of the shear force. The nucleated surface cracks propagated in either the ferrite-cementite interface or pro-eutectoid ferrite-pearlite interface [60]. The surface and subsurface cracks in pearlitic microstructures regularly propagate in the pro-eutectoid ferrite because this phase is more ductile than perlite. The ductility exhaustion of ferrite is faster and allows for the formation of voids in function of the disassociated interface between the softer and the harder phases. This effect also occurs in the ferrite of the pearlite,

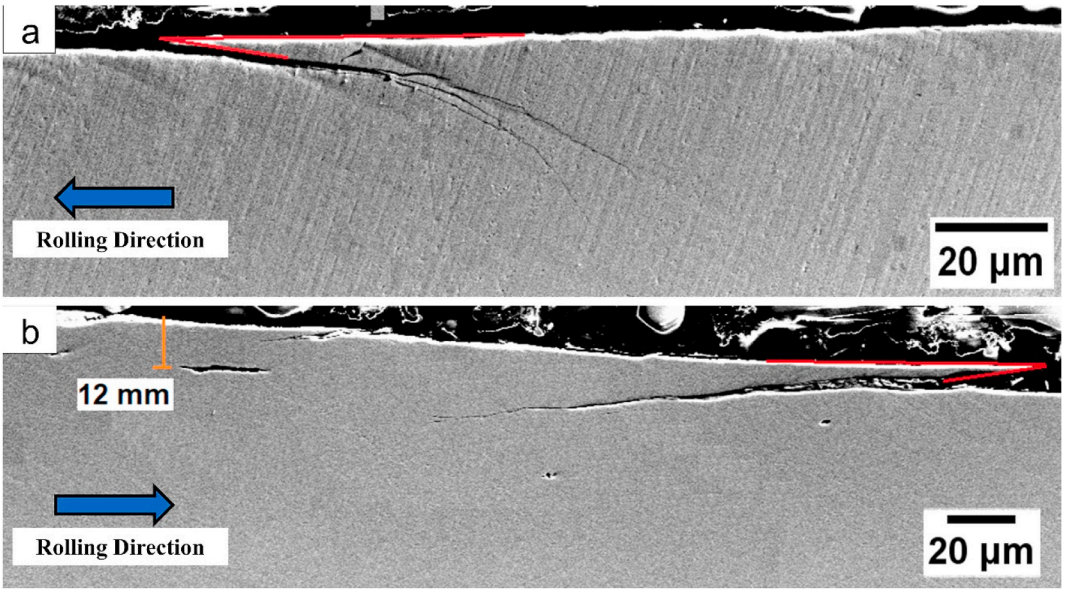

Fig. 13. Cross-section subsurface after 500,000 cycles. a) 7MA; b) 7MB. Scanning electron microscopy (SEM).

Table 3
Characteristics of the cracks found in cross-section images.

Steel	Disc	Range of the angle of surface cracks (°)	Average depth of surface cracks (μm)	The maximum depth of subsurface cracks (μm)
7C	A	7.4–9.8	13 ± 3	15
	B	5.9–7.4	11 ± 2	23
7M	A	6.2–8.6	8 ± 2	10
	B	7.9–11.0	33 ± 3	17

and as the orientation of the pearlite lamella is parallel to the surface owing to the deformation, the cracks have fewer barriers to prevent their spreading [9,60,61].

Figs. 17 and 18 present the chemically attacked cross-sectional view of the 7 M steel discs. Discs 7MA and 7MB showed deformation of the microstructure following the rolling direction, and 7MA subsurface strain appeared shallower than that of 7MB, according to Fig. 10. It can be observed in Fig. 17 that 7MA had the same behavior of the deformed and elongated proeutectoid ferrite because of the action of the shear force. As the initial microstructure was degenerated pearlite (7MA), the microstructure close to the surface was more broken and compacted than 7CA microstructure, providing higher hardness than 7CA. Regarding 7MB, the bainite microstructure close to the surface followed the rolling direction and was broken and well joined. This effect provided higher hardness close to the surface compared to the other discs.

The MBN analyses are illustrated in Fig. 19. The values are the average of 12 measurements taken for 7CB and 7MB each. As a track formed on 7CA and 7MA, MBN was not measured for either of them. The root means square voltage of MBN (MBN_{RMS}) signal had a greater increment in 7MB (167%) than in 7CB (26%). When there is an increment in the MBN_{RMS} values, three possibilities are considered: an increase in the tensile residual stress, a decrease in the hardness, or low plastic deformation [62–65]. In this study, there was an increment in the hardness and plastic deformation, decreasing the MBN_{RMS} values. Conversely, as the MBN_{RMS} values had risen after the tests, the reason

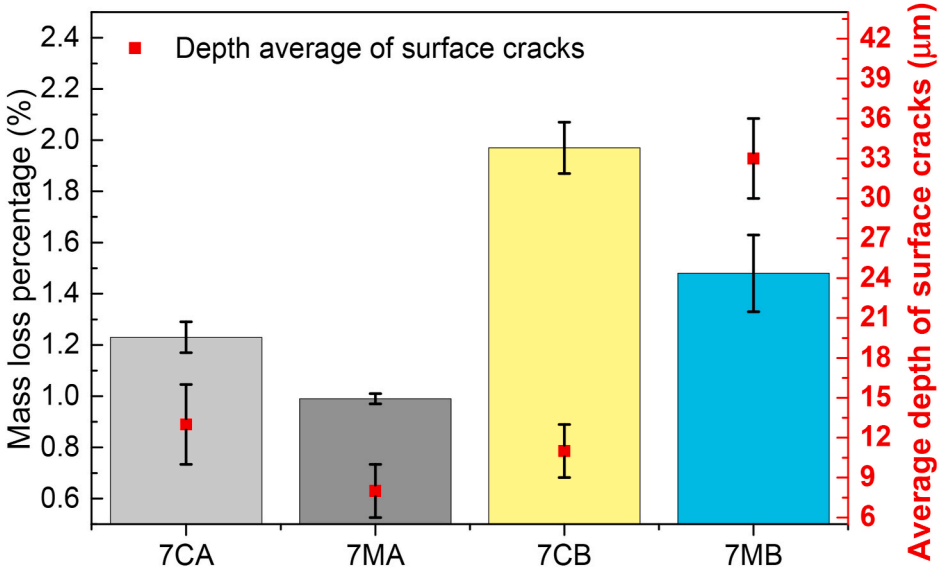

Fig. 14. Correlation between mass loss and surface crack propagation.

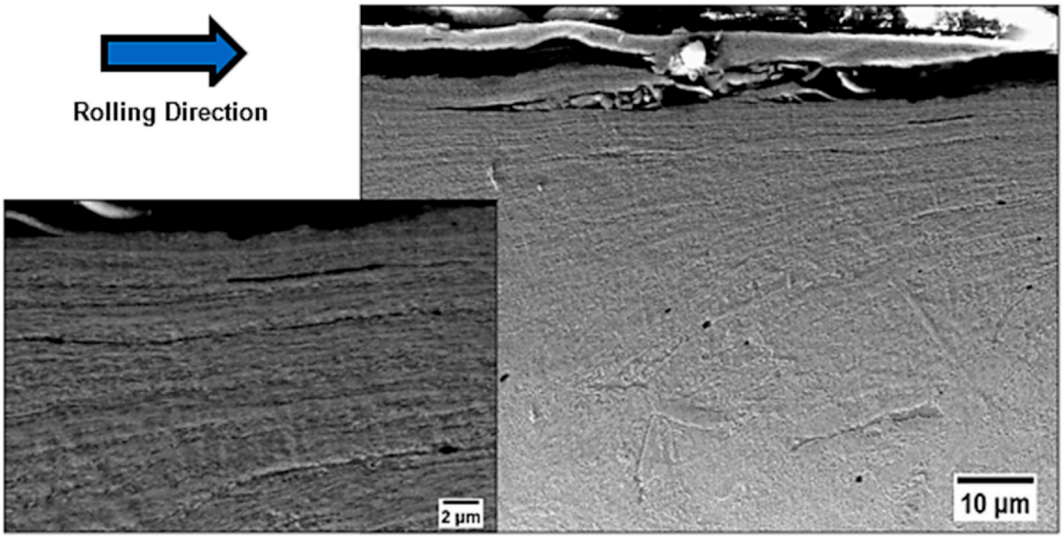

Fig. 15. Scanning electron microscopy (SEM) image of the cross-sectional view of 7CA evidencing plastic deformation. 2% Nital.

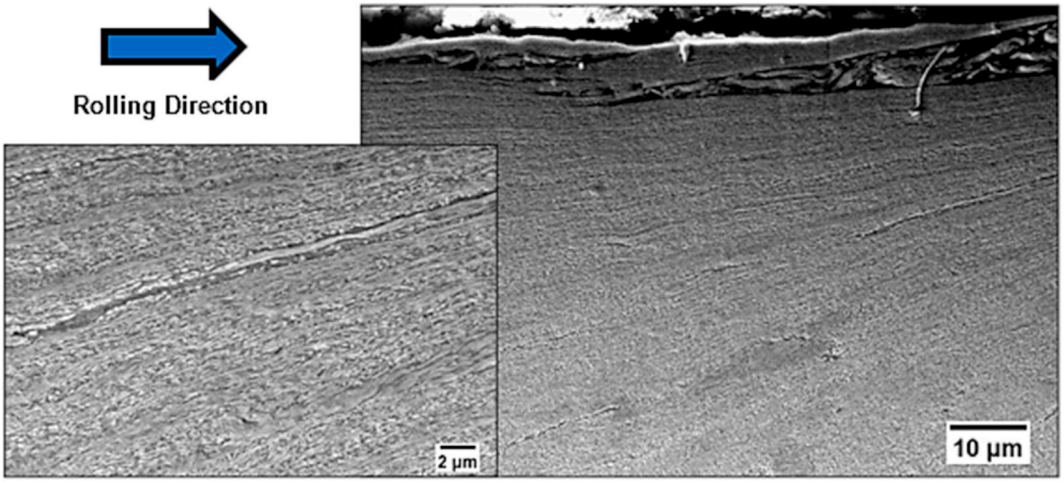

Fig. 16. Scanning electron microscopy (SEM) image of the cross-sectional view of 7CB evidencing plastic deformation. 2% Nital.

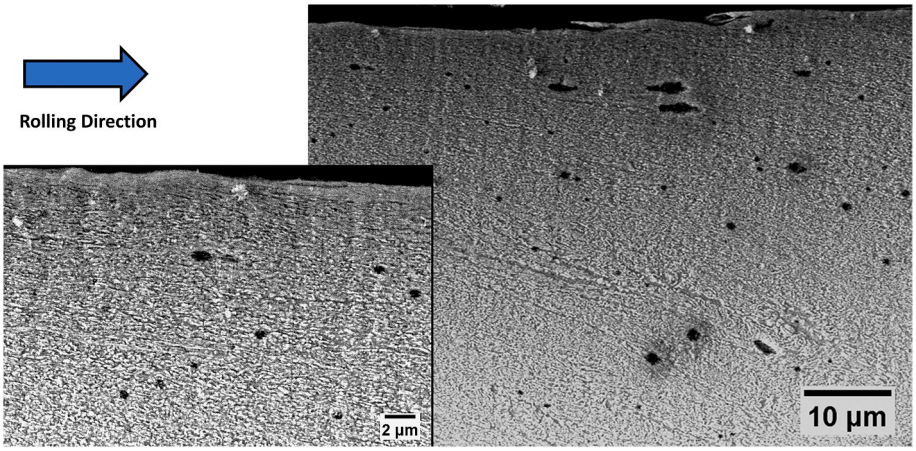

Fig. 17. Scanning electron microscopy (SEM) image of the cross-sectional view of 7MA steel evidencing plastic deformation. 2% Nital.

would be the predominance of increased tensile residual stress. The 40 Hz frequency used in MBN analyses collected the stresses closer to the surface, and the MBN results could be correlated with the deformed layer depth as well as the hardness close to the surface. As in 7MB the deformed layer depth was the shallowest, the contact stresses were absorbed in a smaller area; thus, the residual stress increment was the

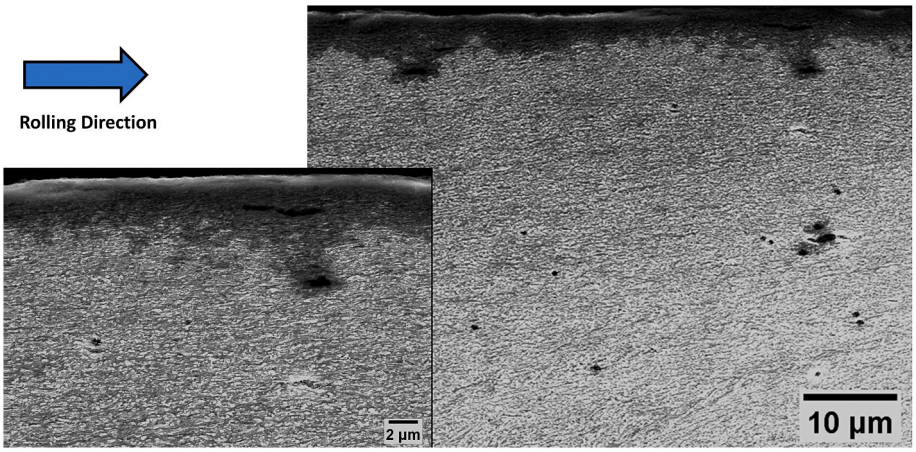

Fig. 18. Scanning electron microscopy (SEM) image of the cross-sectional view of 7MB steel evidencing plastic deformation. 2% Nital.

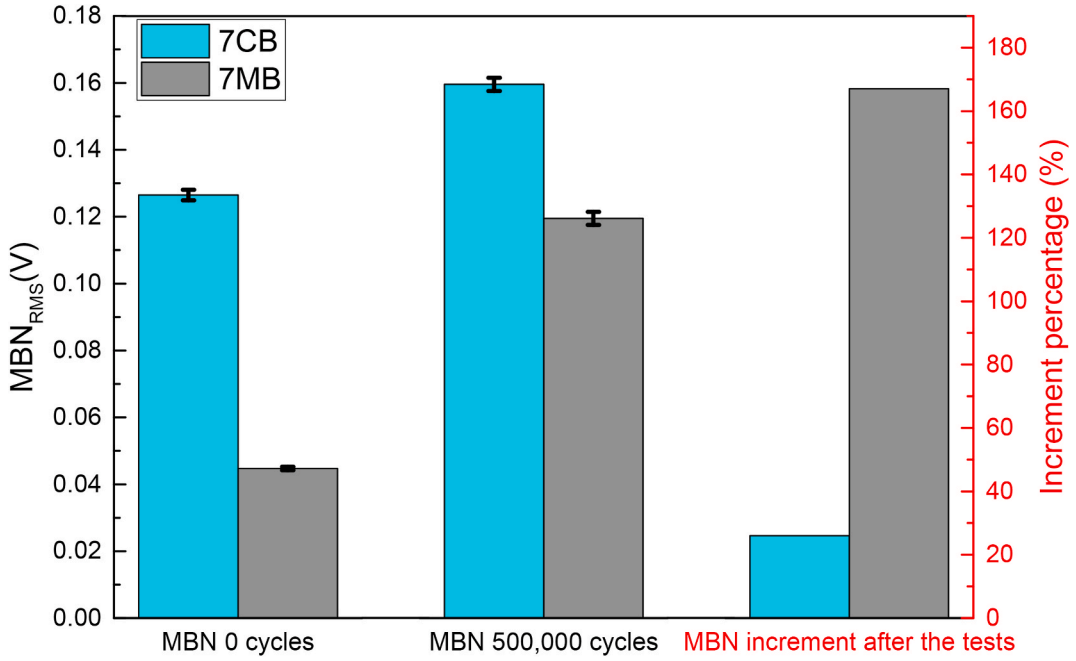

Fig. 19. The average of magnetic Barkhausen noise (MBN) measurements for 7CB and 7MB discs before the tests, after the 500,000 cycles, and their increment percentage.

greatest for this disc. On the other hand, in 7CB the residual stress was higher before the twin-disc tests, as indicated by the higher MBN_{RMS} values. The tensile stress also increased in this disc, but the hardness and deformation increments were greater in it than in 7MB. Although the residual stress increased the MBN values, hardening effects and the initial residual stress limited this increment.

Fig. 20 presents the shakedown diagram of 7C and 7 M steels. It considers the friction coefficient throughout the test in the horizontal axis and the normalized load in the vertical axis. The normalized load is a dimensionless value related to the maximum initial contact pressure (MPa) and to the Yield strength (MPa) [58,66]. As observed, both steels are in the ratcheting zone, which corroborates the results obtained from the surface and subsurface analyses. As 7 M steel is closer to the limit between ratcheting and elastic shakedown state, it was expected that 7 M steel presented the less damaged surface after the tests, according to Fig. 9.

It is worth reporting that these results would be a first verification of the tribological behavior of the class D steel. In this configuration, using the same material to the top and lower discs with exclusively slip of 0.75%, the results showed that 7 M steels presented a better performance than 7C steels. However, it is important to test this material in conditions of curves, which present higher slipping, as well as 7 M steel should be tested against different rail materials, with the materials present in the contact, such as contaminants (water, sand, leaves, etc.) simulating the railway environment, and lubricants (grease and friction modifiers). These additional tests would enable the full knowledge of 7 M steel behavior for all operational conditions of the railway. This way, it would be possible to confirm whether the 7 M steel is a good alternative to be applied in railway wheel steels.

4. Conclusion

After the twin-disc tests performed with class C (7C) and class D (7 M) steels of forged railway wheels, the following conclusions were reached:

- 7 M steel presented better wear performance than 7C steel under the specific small-scale test conditions. This result was due to the higher

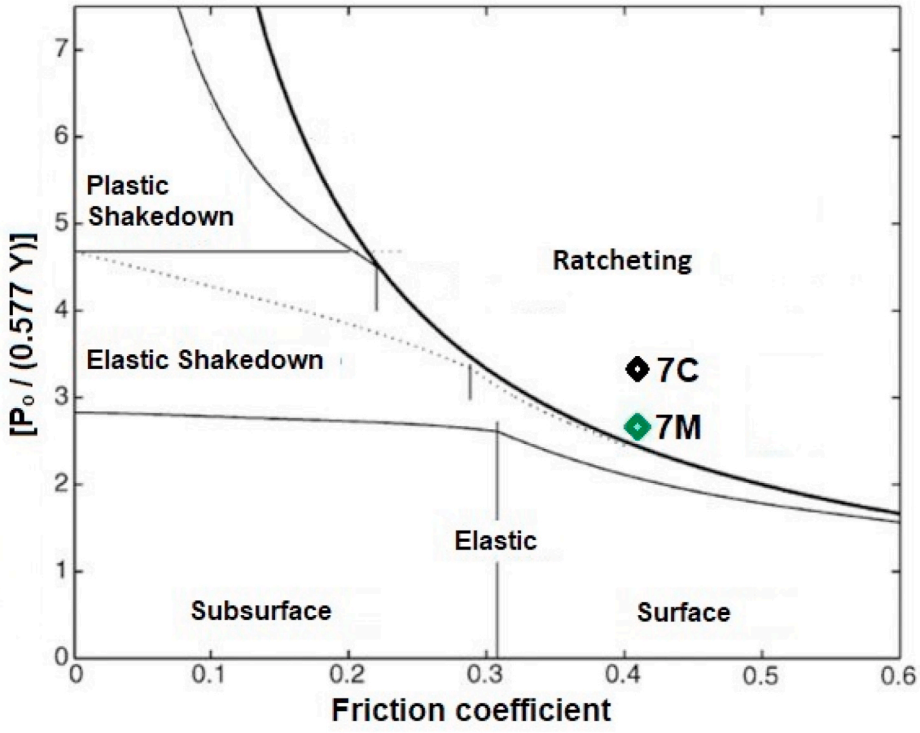

Fig. 20. Shakedown diagram of the steels used in the tests.

initial hardness and the better ability of the 7 M steel microstructure to absorb the high contact stresses evidenced by the increase in MBN values after the tests.

- Both steels operated in the ratcheting zone characterized by cracks and delamination on the surface. 7C steel presented a more deteriorated surface in 7CA and 7CB, which was according to the shakedown map.
- Surface and subsurface cracks were formed in all discs. The surface cracks were deeper in 7MB, and they correlated with the wear behavior. As wear in 7MB was lower, it took longer for the cracks to be removed, so they could propagate longer. The higher wear in 7CB removed the RCF cracks quickly, so the propagation was reduced.
- The microalloyed class D steel indicated better performance than that of the class C steel under direct comparison and specific test conditions. However, additional tests, such as using discs from wheel and rail material with several slip ratios, would be necessary to verify whether 7 M steel is suitable for use in service on railway vehicles.

CRediT authorship contribution statement

A.B. Rezende: Conceptualization, Methodology, Validation, Formal analysis, Investigation, Data curation, Writing - original draft, Writing - review & editing, Visualization. **S.T. Fonseca:** Conceptualization, Methodology, Validation, Writing - review & editing, Supervision, Project administration. **R.S. Miranda:** Investigation, Data curation, Writing - original draft, Writing - review & editing. **F.M. Fernandes:** Data curation, Writing - original draft, Visualization. **F.A.F. Grijalba:** Resources, Writing - review & editing. **P.F.S. Farina:** Resources, Writing - review & editing, Supervision. **P.R. Mei:** Resources, Writing - review & editing, Supervision, Project administration.

Declaration of competing interest

The authors declare that they have no known competing financial interests or personal relationships that could have appeared to influence the work reported in this paper.

Acknowledgments

The authors thank Vale S.A. and the Brazilian National Council for Scientific and Technological Development (CNPQ) (process 140786/2017-1) for their support.

References

[1] J.W. Seo, H.K. Jun, S.J. Kwon, D.H. Lee, Rolling contact fatigue and wear of two different rail steels under rolling-sliding contact, Int. J. Fatig. 83 (2016) 184–194, https://doi.org/10.1016/j.ijfatigue.2015.10.012.

[2] L. Bai, R. Liu, F. Wang, Q. Sun, F. Wang, Estimating railway rail service life: a rail-grid-based approach, Transport. Res. Part A Policy Pract. 105 (2017) 54–65, https://doi.org/10.1016/j.tra.2017.08.007.

[3] T. Reis, E. de A. Lima, F. Bertelli, A.A. dos Santos Junior, Progression of plastic strain on heavy-haul railway rail under random pure rolling and its influence on crack initiation, Adv. Eng. Software 124 (2018) 10–21, https://doi.org/10.1016/j.advengsoft.2018.07.003.

[4] C. peng Liu, R. ming Ren, D. yi Liu, X. juan Zhao, C. huan Chen, An EBSD investigation on the evolution of the surface microstructure of D2 wheel steel during rolling contact fatigue, Tribol. Lett. 68 (2020) 1–11, https://doi.org/10.1007/s11249-020-1277-1.

[5] A. Bevan, P. Molyneux-Berry, B. Eickhoff, M. Burstow, Development and validation of a wheel wear and rolling contact fatigue damage model, Wear 307 (2013) 100–111, https://doi.org/10.1016/j.wear.2013.08.004.

[6] D. Zapata, J. Jaramillo, A. Toro, Rolling contact and adhesive wear of bainitic and pearlitic steels in low load regime, Wear 271 (2011) 393–399, https://doi.org/10.1016/j.wear.2010.10.009.

[7] A.P.G. Chaves, D.M.A. Centeno, M. Masoumi, H. Goldenstein, Effect of the microstructure on the wear resistance of a pearlitic steel, Mater. Res. 23 (2020) 1–8, https://doi.org/10.1590/1980-5373-mr-2019-0605.

[8] D.J. Minicucci, S.T. Fonseca, R.L.V. Boas, H. Goldenstein, P.R. Mei, Development of niobium microalloyed steel for railway wheel with pearlitic bainitic microstructure, Mater. Res. 22 (2019) 8, https://doi.org/10.1590/1980-5373-mr-2019-0324.

[9] C. Liu, R. Ren, D. Zhao, C. Chen, An EBSD investigation on the evolution of the surface microstructure of D2 wheel steel during rolling contact fatigue, Tribol. Lett. 68 (2020) 11, https://doi.org/10.1007/s11249-020-1277-1.

[10] Q. Li, J. Guo, A. Zhao, Effect of upper bainite on wear behaviour of high-speed wheel steel, Tribol. Lett. 67 (2019) 1–9, https://doi.org/10.1007/s11249-019-1239-7.

[11] A. Ekberg, B. Åkesson, E. Kabo, Wheel/rail rolling contact fatigue - probe, predict, prevent, Wear 314 (2014) 2–12, https://doi.org/10.1016/j.wear.2013.12.004.

[12] F.C. Robles Hernández, S. Cummings, S. Kalay, D. Stone, Properties and microstructure of high performance wheels, Wear 271 (2011) 374–381, https://doi.org/10.1016/j.wear.2010.10.017.

[13] R. Ordóñez Olivares, C.I. Garcia, A. DeArdo, S. Kalay, F.C. Robles Hernández, Advanced metallurgical alloy design and thermomechanical processing for rails steels for North American heavy haul use, Wear 271 (2011) 364–373, https://doi.org/10.1016/J.WEAR.2010.10.048.

[14] A.P.A. Cunha, R.L. Villas Bôas, S.T. Fonseca, P.R. Mei, Effect of microalloying on structure and properties of hot rolled 0.5 %C steel, J. Metall. Eng. 2 (2013), 0–6.

[15] D. Zeng, L. Lu, N. Zhang, Y. Gong, J. Zhang, Effect of different strengthening methods on rolling/sliding wear of ferrite–pearlite steel, Wear 358–359 (2016) 62–71, https://doi.org/10.1016/J.WEAR.2016.04.003.

[16] S.T. Fonseca, A. Sinatora, A.J. Ramirez, D.J. Minicucci, C.R. Afonso, P.R. Mei, Effects of vanadium on the continuous cooling transformation of 0.7 %C steel for railway wheels, Defect Diffusion Forum 367 (2016) 60–67. https://doi.org/10.4028/www.scientific.net/DDF.367.60.

[17] A.B. Rezende, G.A. Amorim, D.J. Minicucci, S.T. Fonseca, P.R. Mei, Effect of vanadium addition on the surface roughness and fatigue crack propagation in a railroad wheel using twin disc wear test, Defect Diffusion Forum 391 (2019) 66–73. https://doi.org/10.4028/www.scientific.net/ddf.391.66.

[18] J. Zhao, Z. Jiang, Thermomechanical processing of advanced high strength steels, Prog. Mater. Sci. 94 (2018) 174–242, https://doi.org/10.1016/j.pmatsci.2018.01.006.

[19] W. Solano-Alvarez, M.J. Peet, E.J. Pickering, J. Jaiswal, A. Bevan, H.K.D. H. Bhadeshia, Synchrotron and neural network analysis of the influence of composition and heat treatment on the rolling contact fatigue of hypereutectoid pearlitic steels, Mater. Sci. Eng. A. 707 (2017) 259–269, https://doi.org/10.1016/j.msea.2017.09.045.

[20] D. Zeng, L. Lu, Y. Gong, N. Zhang, Y. Gong, Optimization of strength and toughness of railway wheel steel by alloy design, Mater. Des. 92 (2016) 998–1006, https://doi.org/10.1016/j.matdes.2015.12.096.

[21] C. Qiu, J. Cookson, P. Mutton, The role of microstructure and its stability in performance of wheels in heavy haul service, J. Mod. Transp. 25 (2017) 261–267, https://doi.org/10.1007/s40534-017-0143-9.

[22] C. Chattopadhyay, S. Sangal, K. Mondal, A. Garg, Improved wear resistance of medium carbon microalloyed bainitic steels, Wear 289 (2012) 168–179, https://doi.org/10.1016/J.WEAR.2012.03.005.

[23] W. Solano-Alvarez, E.J. Pickering, H.K.D.H. Bhadeshia, Degradation of nanostructured bainitic steel under rolling contact fatigue, Mater. Sci. Eng. A. 617 (2014) 156–164, https://doi.org/10.1016/J.MSEA.2014.08.071.

[24] S. Sharma, S. Sangal, K. Mondal, Wear behaviour of bainitic rail and wheel steels, Mater. Sci. Technol. 32 (2016) 266–274, https://doi.org/10.1080/02670836.2015.1112537.

[25] S. Sharma, S. Sangal, K. Mondal, Reciprocating sliding wear behavior of newly developed bainitic steels, Metall. Mater. Trans. A Phys. Metall. Mater. Sci. 45 (2014) 5451–5468, https://doi.org/10.1007/s11661-014-2507-7.

[26] O.A. Zambrano, J.A. Gómez, J.J. Coronado, S.A. Rodríguez, The sliding wear behaviour of steels with the same hardness, Wear 418–419 (2019) 201–207, https://doi.org/10.1016/j.wear.2018.12.002.

[27] W. Solano-Alvarez, L. Fernandez Gonzalez, H.K.D.H. Bhadeshia, The effect of vanadium alloying on the wear resistance of pearlitic rails, Wear (2019) 436–437, https://doi.org/10.1016/j.wear.2019.203004, 203004.

[28] J.J. Coronado, S.A. RodrÍguez, Cementite characterization with chromium and vanadium contents using indentation technique, J. Iron Steel Res. Int. 22 (2015) 366–370, https://doi.org/10.1016/S1006-706X(15)30013-3.

[29] I.R. Shein, N.I. Medvedeva, A.L. Ivanovskii, Electronic structure and magnetic properties of Fe3C with 3d and 4d impurities, Phys. Status Solidi Basic Res. 244 (2007) 1971–1981, https://doi.org/10.1002/pssb.200642400.

[30] L.B. Godefroid, L.P. Moreira, T.C.G. Vilela, G.L. Faria, L.C. Candido, E.S. Pinto, Effect of chemical composition and microstructure on the fatigue crack growth resistance of pearlitic steels for railroad application, Int. J. Fatig. 120 (2019) 241–253, https://doi.org/10.1016/j.ijfatigue.2018.10.016.

[31] A.A.R. "Association of American Railroad", Manual of Standards and Recommended Practices, section G, M-107/M208, appendix C, topic 3.1.6, vol. 1, 2011, p. 180.

[32] R. Galas, D. Smejkal, M. Omasta, M. Hartl, Twin-disc experimental device for study of adhesion in wheel-rail contact, Eng. Mech. 21 (2014) 329–334.

[33] W.R. Tyfour, J.H. Beynon, A. Kapoor, Deterioration of rolling contact fatigue life of pearlitic rail steel due to dry-wet rolling-sliding line contact, Wear 197 (1996) 255–265, https://doi.org/10.1016/0043-1648(96)06978-5.

[34] A.B. Rezende, S.T. Fonseca, F.M. Fernandes, R.S. Miranda, F.A.F. Grijalba, P.F. S. Farina, R. Mei, Wear behavior of bainitic and pearlitic microstructures from microalloyed railway wheel steel, Wear 456–457 (2020) 203377, https://doi.org/10.1016/j.wear.2020.203377.

[35] S.T. da Fonseca, Efeito de adições de vanádio, nióbio e molibdênio na estrutura e propriedades mecânicas de aços com 0,7 % C utilizados na fabricação de rodas ferroviárias, Tese (Doutorado), Universidade Estadual de Campinas, 2015.

[36] L.G. de Oliveira, Influência Do Processo De Fabricação No Comportamento Mecânico De Rodas Ferroviárias, Tese (Doutorado), Universidade Estadual Paulista, 2013.

[37] P.C. Liu, Z.X. Wang, J.H. Cong, R.D.K. Misra, X.M. Wang, A.M. Guo, Y.Q. Zhang, The significance of Nb interface segregation in governing pearlitic refinement in high carbon steels, Mater. Lett. 279 (2020) 128520, https://doi.org/10.1016/j.matlet.2020.128520.

[38] Z. Li, Q. Yong, Z. Zhang, X. Sun, J. Cao, H. Qi, Z. Liao, Microstructure evolution during continuous cooling in niobium microalloyed high carbon steels, Met. Mater. Int. 20 (2014) 801–806, https://doi.org/10.1007/s12540-014-5001-2.

[39] A.B. Rezende, F.M. Fernandes, S.T. Fonseca, P.F.S. Farina, H. Goldenstein, P. R. Mei, Effect of alloy elements in time temperature transformation diagrams of railway wheels, Defect Diffusion Forum 400 (2020) 11–20.

[40] H. Hu, G. Xu, L. Wang, Z. Xue, Y. Zhang, G. Liu, The effects of Nb and Mo addition on transformation and properties in low carbon bainitic steels, Mater. Des. 84 (2015) 95–99, https://doi.org/10.1016/j.matdes.2015.06.133.

[41] W.T. Zhu, L.C. Guo, L.B. Shi, Z.B. Cai, Q.L. Li, Q.Y. Liu, W.J. Wang, Wear and damage transitions of two kinds of wheel materials in the rolling-sliding contact, Wear 398–399 (2018) 79–89, https://doi.org/10.1016/j.wear.2017.11.023.

[42] Y. Zhou, J.F. Peng, W.J. Wang, X.S. Jin, M.H. Zhu, Slippage effect on rolling contact wear and damage behavior of pearlitic steels, Wear 362–363 (2016) 78–86, https://doi.org/10.1016/j.wear.2016.05.001.

[43] S. Das Bakshi, A. Leiro, B. Prakash, H.K.D.H. Bhadeshia, Dry rolling/sliding wear of nanostructured bainite, Wear 316 (2014) 70–78, https://doi.org/10.1016/J.WEAR.2014.04.020.

[44] R. Halama, R. Fajkoš, P. Matušek, P. Bábková, F. Fojtík, L. Václavek, Contact defects initiation in railroad wheels - experience, experiments and modelling, Wear 271 (2011) 174–185, https://doi.org/10.1016/j.wear.2010.10.053.

[45] Q. Li, X. Huang, W. Huang, Fatigue property and microstructure deformation behavior of multiphase microstructure in a medium-carbon bainite steel under rolling contact condition, Int. J. Fatig. 125 (2019) 381–393, https://doi.org/10.1016/j.ijfatigue.2019.04.019.

[46] S.M. Hasan, D. Chakrabarti, S.B. Singh, Dry rolling/sliding wear behaviour of pearlitic rail and newly developed carbide-free bainitic rail steels, Wear 408–409 (2018) 151–159, https://doi.org/10.1016/J.WEAR.2018.05.006.

[47] C. Hardwick, R. Lewis, R. Stock, The effects of friction management materials on rail with pre existing rcf surface damage, Wear 384–385 (2017) 50–60, https://doi.org/10.1016/j.wear.2017.04.016.

[48] S. Maya-Johnson, J. Felipe Santa, A. Toro, Dry and lubricated wear of rail steel under rolling contact fatigue - wear mechanisms and crack growth, Wear 380–381 (2017) 240–250, https://doi.org/10.1016/j.wear.2017.03.025.

[49] K.L. Johnson, Contact Mechanics, Cambridge University Press, 1985.

[50] P. Christoforou, D.I. Fletcher, R. Lewis, Benchmarking of premium rail material wear, Wear 436–437 (2019) 202990, https://doi.org/10.1016/j.wear.2019.202990.

[51] J.P. Liu, Y.Q. Li, Q.Y. Zhou, Y.H. Zhang, Y. Hu, L.B. Shi, W.J. Wang, F.S. Liu, S. B. Zhou, C.H. Tian, New insight into the dry rolling-sliding wear mechanism of carbide-free bainitic and pearlitic steel, Wear 432–433 (2019) 202943, https://doi.org/10.1016/j.wear.2019.202943.

[52] X. Shi, Q. Yan, X. Zhang, G. Diao, C. Zhang, Z. Hong, Z. Wen, X. Jin, Hardness matching of rail/wheel steels for high-speed-train based on wear rate and rolling contact fatigue performance, Mater. Res. Express 6 (2019), https://doi.org/10.1088/2053-1591/ab072d.

[53] L. Ma, C.G. He, X.J. Zhao, J. Guo, Y. Zhu, W.J. Wang, Q.Y. Liu, X.S. Jin, Study on wear and rolling contact fatigue behaviors of wheel/rail materials under different slip ratio conditions, Wear 366–367 (2016) 13–26, https://doi.org/10.1016/J.WEAR.2016.04.028.

[54] G. Donzella, A. Mazzù, C. Petrogalli, Competition between wear and rolling contact fatigue at the wheel—rail interface: some experimental evidence on rail steel, Proc. Inst. Mech. Eng. - Part F J. Rail Rapid Transit 223 (2009) 31–44, https://doi.org/10.1243/09544097JRRT161.

[55] A. Leiro, A. Kankanala, E. Vuorinen, B. Prakash, Tribological behaviour of carbide-free bainitic steel under dry rolling/sliding conditions, Wear 273 (2011) 2–8, https://doi.org/10.1016/j.wear.2011.03.025.

[56] S.K. Dhua, A. Ray, S.K. Sen, M.S. Prasad, K.B. Mishra, S. Jha, Influence of nonmetallic inclusion characteristics on the mechanical properties of rail steel, J. Mater. Eng. Perform. 9 (2000) 700–709, https://doi.org/10.1361/105994900770345584.

[57] G. Tressia, A. Sinatora, H. Goldenstein, M. Masoumi, Improvement in the wear resistance of a hypereutectoid rail via heat treatment, Wear 442–443 (2020) 203122, https://doi.org/10.1016/J.WEAR.2019.203122.

[58] F. Salas Vicente, M. Pascual Guillamón, Use of the fatigue index to study rolling contact wear, Wear 436–437 (2019) 203036, https://doi.org/10.1016/j.wear.2019.203036.

[59] H. Chen, C. Zhang, W. Liu, Q. Li, H. Chen, Z. Yang, Y. Weng, Microstructure evolution of a hypereutectoid pearlite steel under rolling-sliding contact loading, Mater. Sci. Eng. A. 655 (2016) 50–59, https://doi.org/10.1016/j.msea.2015.12.082.

[60] Q.H. Li, C. Zhang, H. Chen, H. Chen, Z. gang Yang, Microstructural evolution of a hypoeutectoid pearlite steel under rolling-sliding contact loading, J. Iron Steel Res. Int. 23 (2016) 1054–1060, https://doi.org/10.1016/S1006-706X(16)30157-1.

[61] M. Masoumi, E.A. Ariza, A. Sinatora, H. Goldenstein, Role of crystallographic orientation and grain boundaries in fatigue crack propagation in used pearlitic rail steel, Mater. Sci. Eng. A. 722 (2018) 147–155, https://doi.org/10.1016/J.MSEA.2018.03.028.

[62] C.H. Gur, Review of residual stress measurement by magnetic barkhausen noise technique, Mater. Perform. Charact. 7 (2018) 504–526, https://doi.org/10.1520/mpc20170080.

[63] F.A. Franco, M.F.R. González, M.F. De Campos, L.R. Padovese, Relation between magnetic barkhausen noise and hardness for jominy quench tests in SAE 4140 and 6150 steels, J. Nondestr. Eval. 32 (2013) 93–103, https://doi.org/10.1007/s10921-012-0162-8.

[64] L. Piotrowski, B. Augustyniak, M. Chmielewski, I. Tomáš, The influence of plastic deformation on the magnetoelastic properties of the CSN12021 grade steel, J. Magn. Magn Mater. 321 (2009) 2331–2335, https://doi.org/10.1016/J.JMMM.2009.02.028.

[65] J.A. Perez-Benitez, J. Capo-Sanchez, J. Anglada-Rivera, L.R. Padovese, A study of plastic deformation around a defect using the magnetic Barkhausen noise in ASTM 36 steel, NDT E Int. 41 (2008) 53–58, https://doi.org/10.1016/J.NDTEINT.2006.12.002.

[66] M. Abdel-Karim, Shakedown of complex structures according to various hardening rules, Int. J. Pres. Ves. Pip. 82 (2005) 427–458, https://doi.org/10.1016/j.ijpvp.2005.01.007.